Joint Energy Harvesting and Communication Analysis for Perpetual Wireless Nanosensor Networks in the Terahertz Band

Josep Miquel Jornet, *Student Member, IEEE*, and Ian F. Akyildiz, *Fellow, IEEE*

***Abstract*—Wireless nanosensor networks (WNSNs) consist of nanosized communicating devices, which can detect and measure new types of events at the nanoscale. WNSNs are the enabling technology for unique applications such as intrabody drug delivery systems or surveillance networks for chemical attack prevention. One of the major bottlenecks in WNSNs is posed by the very limited energy that can be stored in a nanosensor mote in contrast to the energy that is required by the device to communicate. Recently, novel energy harvesting mechanisms have been proposed to replenish the energy stored in nanodevices. With these mechanisms, WNSNs can overcome their energy bottleneck and even have infinite lifetime (perpetual WNSNs), provided that the energy harvesting and consumption processes are jointly designed. In this paper, an energy model for self-powered nanosensor motes is developed, which successfully captures the correlation between the energy harvesting and the energy consumption processes. The energy harvesting process is realized by means of a piezoelectric nanogenerator, for which a new circuital model is developed that can accurately reproduce existing experimental data. The energy consumption process is due to the communication among nanosensor motes in the terahertz band (0.1–10 THz). The proposed energy model captures the dynamic network behavior by means of a probabilistic analysis of the total network traffic and the multiuser interference. A mathematical framework is developed to obtain the probability distribution of the nanosensor mote energy and to investigate the end-to-end successful packet delivery probability, the end-to-end packet delay, and the achievable throughput of WNSNs. Nanosensor motes have not been built yet and, thus, the development of an analytical energy model is a fundamental step toward the design of WNSNs architectures and protocols.**

***Index Terms*—Energy harvesting, graphene, nanonetworks, nanosensors, nanowires, terahertz band.**

Manuscript received December 4, 2011; accepted January 19, 2012. Date of publication January 31, 2012; date of current version May 9, 2012. This work was supported by the Fundación Caja Madrid. The review of this paper was arranged by Associate Editor P. J. Burke.

J. M. Jornet is with the Broadband Wireless Networking Laboratory, School of Electrical and Computer Engineering, Georgia Institute of Technology, Atlanta, GA 30332 USA (e-mail:jmjornet@ece.gatech.edu).

I. F. Akyildiz is with the Broadband Wireless Networking Laboratory, School of Electrical and Computer Engineering, Georgia Institute of Technology, Atlanta, GA 30332 USA, with the NaNoNetworking Center in Catalunya (N3Cat), Universitat Politècnica de Catalunya, 08034 Barcelona, Spain (e-mail: ian@ece.gatech.edu).

Color versions of one or more of the figures in this paper are available online at http://ieeexplore.ieee.org.

Digital Object Identifier 10.1109/TNANO.2012.2186313

I. Introduction

NANOTECHNOLOGY is providing a new set of tools to the engineering community to design and manufacture novel devices just a few hundred nanometers in size. One of the early applications of these nanodevices is in the field of nanosensing [26], [40]. Nanosensors are not just tiny sensors, but devices that take advantage of the properties of novel nanomaterials to identify and measure new types of events in the nanoscale, such as chemical compounds in concentrations as low as one part per billion [29], or the presence of virus or harmful bacteria [39]. However, the sensing range of a nanosensor is usually limited to its close nanoenvironment. Moreover, an external device and the user interaction are necessary to read the actual measurement of the nanosensor.

The development of an autonomous nanosensor mote with communication capabilities will overcome the limitations of individual nanosensors and expand their potential applications [1]–[3]. Wireless nanosensor networks (WNSNs) will enable advanced applications of nanotechnology in the biomedical field (e.g., intrabody health monitoring and drug delivery systems), in environmental research (e.g., distributed air pollution control), and in defense and military technology (e.g., surveillance against new types of nuclear, biological and chemical attacks at the nanoscale). To enable these applications, nanosensor motes require minimal power, data storage, processing, and communication capabilities.

A major challenge in WNSNs is posed by the very limited energy storage capacity of nanosensor motes. Novel energy harvesting mechanisms have been recently proposed as a way to replenish the energy of nanodevices [5], [6], [34], [37], [38]. For example, in [37], a piezoelectric nanogenerator is demonstrated experimentally. In the presented design, an array of zinc oxide (ZnO) nanowires is used to power a commercial laser diode (LD). The waiting time to power the LD just for a few milliseconds is in the order of 10 min when a 50-Hz vibration is applied to the nanowires. Note that the energy harvesting systems of nanosensor motes are much more limiting than those of microscale sensor motes [32], both due to the extremely limited capacity of nanobatteries and the low rate at which energy can be harvested.

The lifetime of energy harvesting networks can tend to infinity provided that the energy harvesting and the energy consumption processes are jointly designed [8], [19]. In contrast to the classical battery-powered devices, the energy of the self-powered devices does not just decrease until the battery is empty, but

it has both positive and negative fluctuations. These variations are not captured in classical energy models [31], [33]. Even in several recent models for energy harvesting networks [16], [18], [21], [30], the correlation between the energy harvesting and the energy consumption processes are not fully captured. In particular, existing models usually assume constant energy harvesting and transmission rates. However, it is reasonable to consider that if a nanodevice fully deplenishes its battery and cannot respond to a communication request, the transmitting nanodevice will attempt to retransmit. This increases the overall network traffic, the multiuser interference and it ultimately has an impact in the energy of the transmitting nanosensor mote and the neighboring nanodevices.

In this paper, we propose an energy model for self-powered nanosensor motes. This model considers both the energy harvesting process by means of a piezoelectric nanogenerator and the energy consumption process due to electromagnetic (EM) communication in the terahertz band (0.1–10 THz) [10], [11], [14]. This model allows us to compute the probability distribution of the nanosensor mote energy and to investigate its variations as function of several system and network parameters. To the best of our knowledge, integrated nanosensor motes have not been built yet and, thus, it is not possible to have experimental measurements of the energy fluctuations in nanosensor motes. Therefore, an analytical energy model is an essential step toward the design of future nanosensor motes as well as WNSNs architectures and protocols.

The main contributions of this paper are summarized as follows. First, we develop an analytical model for the energy harvesting process of a nanosensor mote powered by a piezoelectric nanogenerator. In addition, realistic numbers are provided for both the energy capacity, i.e., the maximum energy that can be stored in an ultra-nanocapacitor, and the energy rate, i.e., the speed at which the energy is scavenged by the system. The new energy harvesting model, the energy capacity, and the energy rate are detailed in Section II.

Second, we review the energy consumption process due to communication among nanosensor motes when a graphene-based nanotransceiver for terahertz band communication is used [1]. For this, we consider our recently proposed communication mechanism for nanosensor motes [11], which is based on the exchange of femtosecond-long pulses. The impact of terahertz band propagation effects, such as molecular absorption loss and noise are captured in our analysis. The energy consumption process is treated in Section III.

Third, we model the fluctuations in the nanosensor mote energy by taking into account the proposed piezoelectric nanogenerator model and the energy consumption due to communication in the terahertz band. Moreover, the proposed model captures the dynamic network behavior by means of a probabilistic analysis of the overall network traffic and multiuser interference. The outcome of this analysis is the probability density function of the nanosensor mote energy as a function several system parameters. The model is presented in Section IV. We then validate it by simulation and we use it to analyze the impact of the energy fluctuations on the WNSN performance in Section V. We conclude this paper in Section VI.

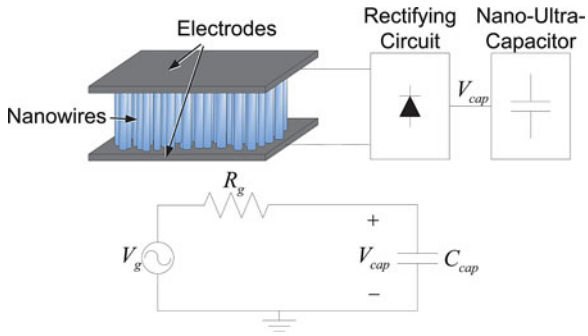

Fig. 1. Piezoelectric nanogenerator (top) and its equivalent model (bottom).

II. Energy Harvesting With Piezoelectric Nanogenerators

Conventional energy harvesting mechanisms, e.g., solar energy, wind power, or underwater turbulences [23], [32], cannot be utilized in WNSNs. For example, the efficiency of photovoltaic nanocells for solar energy harvesting is extremely low even if novel nanocomponents such as carbon nanotubes are used to improve their sensitivity [15]. In addition, in many of the applications of WNSNs, sunlight is not available. Moreover, classical mechanisms to harvest kinetic energy from wind or underwater turbulences are not feasible in the nanoscale due to the technology limitations [1].

A pioneering mechanism to power nanosensor motes is to harvest vibrational energy by exploiting the piezoelectric effect of ZnO nanowires [34]. A piezoelectric nanogenerator, shown in Fig. 1, consists of 1) an array of ZnO nanowires, 2) a rectifying circuit, and 3) a ultra-nanocapacitor. When the nanowires are bent or compressed, an electric current is generated between the ends of the nanowires. This current is used to charge a capacitor. When the nanowires are released, an electric current in the opposite direction is generated and used to charge the capacitor after proper rectification. The compress-release cycles of the nanowires are created by an external energy source, e.g., ambient vibrations or artificially generated ultrasonic waves [34].

Piezoelectric nanogenerators have been prototyped in [37] and [38]. In [37], a very dense array of vertically aligned ZnO nanowires is used to power an LD for the transmission of a very short pulse. In [38], both the vertical and lateral integration of a large number of ZnO nanowires in an array is demonstrated and used to power a nanowire pH sensor and a nanowire UV sensor. However, there is no analytical model for the energy capacity and the harvesting rate of these nanogenerators. Only the fundamental limits of a single nanowire were analytically explored in [7], but a system-level model that captures the effect of the rectifying circuit and the capacitor is missing.

In this section, we develop an analytical model for piezoelectric nanogenerators that captures the fundamental principles, capabilities, and limitations of the energy harvesting process. In addition, we compare our analytical results with the experimental measurements in [37] and we determine realistic values for the energy capacity and the energy harvesting rate.

A. General Model for Piezoelectric Nanogenerators

As shown in Fig. 1, we model a piezoelectric nanogenerator as a nonideal current source composed by an ideal voltage source V_g in series with a resistor R_g. The generator voltage V_g corresponds to the electrostatic potential of a bent nanowire minus the voltage dropped in the rectifying circuit. The value of the resistor is $R_g = V_g/I_g$, where I_g stands for the generator current. This is defined as $I_g = \Delta Q/t_{\text{cycle}}$, where ΔQ is the amount of electric charge, or harvested charge, obtained from a single compress-release cycle of the nanowire array and t_{cycle} is the cycle length.

The voltage V_{cap} of the charging capacitor can be computed as a function of the number of cycles n_{cycle}:

$$V_{\text{cap}}\left(n_{\text{cycle}}\right) = V_g\left(1 - e^{\left(-\frac{n_{\text{cycle}} t_{\text{cycle}}}{R_g C_{\text{cap}}}\right)}\right) = V_g\left(1 - e^{\left(-\frac{n_{\text{cycle}} \Delta Q}{V_g C_{\text{cap}}}\right)}\right) \quad (1)$$

where t_{cycle} is the cycle length, R_g is the resistor of the nonideal source, and C_{cap} is the total capacitance of the ultra-nanocapacitor. V_g is the generator voltage and ΔQ is the harvested charge per cycle, which are determined by the nanowire array. In this computation we do not take into account the leakage in the nanocapacitor [42] due to the fact that these values have yet not been quantified and are expectedly very low [25].

The energy stored in the capacitor E_{cap} can be computed as a function of the number of cycles n_{cycle}:

$$E_{\text{cap}}\left(n_{\text{cycle}}\right) = \frac{1}{2} C_{\text{cap}}\left(V_{\text{cap}}\left(n_{\text{cycle}}\right)\right)^2 \quad (2)$$

where C_{cap} is the total capacitance of the ultra-nanocapacitor and V_{cap} is computed from (1). The energy capacity $E_{\text{cap}-\max}$, which is defined as the maximum energy stored in the ultra-nanocapacitor, corresponds to

$$E_{\text{cap}-\max} = \max\{E_{\text{cap}}\left(n_{\text{cycle}}\right)\} = \frac{1}{2} C_{\text{cap}} V_g^2 \quad (3)$$

where C_{cap} is the total capacitance of the ultra-nanocapacitor and V_g is the generator voltage.

The number of cycles n_{cycle} needed to charge the ultra-nanocapacitor up to an energy value E is then

$$n_{\text{cycles}}\left(E\right) = \left\lceil -\frac{V_g C_{\text{cap}}}{\Delta Q} \ln\left(1 - \sqrt{\frac{2E}{C_{\text{cap}} V_g^2}}\right)\right\rceil \quad (4)$$

where V_g is the generator voltage, C_{cap} refers to the ultra-nanocapacitor capacitance, ΔQ is the harvested charge per cycle, and V_g is generator voltage. The operator $\lceil \cdot \rceil$ returns the lowest integer number which is higher than the operand.

Finally, the energy harvesting rate λ_e in Joule/second at which the ultra-nanocapacitor is charged can be computed as a function of the current energy in the ultra-nanocapacitor E_{cap} (2) and the increase in the energy of the capacitor ΔE:

$$\lambda_e\left(E_{\text{cap}}, \Delta E\right) = \left(\frac{n_{\text{cycle}}}{t_{\text{cycle}}}\right) \cdot \frac{\Delta E}{n_{\text{cycle}}\left(E_{\text{cap}} + \Delta E\right) - n_{\text{cycle}}\left(E_{\text{cap}}\right)} \quad (5)$$

where n_{cycle} is the number of cycles given by (4) and t_{cycle} refers to the time between consecutive cycles.

If the compress-release cycles are created by an artificially generated ultrasonic wave, t_{cycle} is constant and corresponds to the inverse of the frequency of the ultrasonic wave. If the compress-release cycles are created by an ambient vibration, the time t_{cycle} is the time between arrivals of a random process. For common vibration sources such as the vents of the air conditioning system of an office or the foot steps on a wooden deck, these arrivals *follow a Poisson distribution* [28].

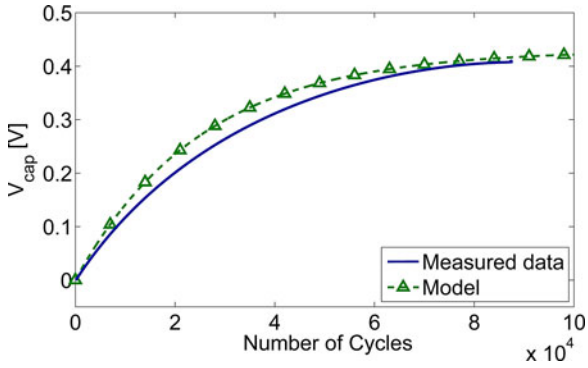

Fig. 2. Comparison between the measured voltage in the capacitor V_{cap} as a function of the number of cycles n_{cycle} reported in [37] and the numerical results for V_{cap} given by our analytical model in (1).

The numerical results obtained with this analytical solution accurately match the measurements reported in [37]. In that experimental setup, a total charge per cycle ΔQ= 3.63 nC is measured. This is used to charge an array of eight microcapacitors with total capacitance C_{cap}=166 μF at a voltage V_g= 0.42 V. In Fig. 2, the voltage in the capacitor V_{cap} as a function of the number of cycles n_{cycle} reported in [37] is compared to the numerical results for V_{cap} given by our analytical model in (1). The proposed model for the voltage of the capacitor V_{cap} accurately matches the measurements.

B. Tailored Model for Nanosensor Motes

The size of the piezoelectric nanogenerators that are prototyped in [37] and [38] is in the order of 10 mm^2. However, the target size of an integrated nanosensor mote is in between 10 and 1000 μm^2 [1]–[3]. Therefore, we need to determine realistic values for the amount of electric charge harvested per cycle ΔQ and the capacitance of the ultra-nanocapacitor C_{cap}, in order to compute the energy capacity $E_{\text{cap}-\max}$ in (3) and the energy harvesting rate λ_e in (5).

The electric charge harvested per cycle ΔQ depends on the size of the nanowire array and the efficiency of the harvesting process. Based on the results in [38], a ΔQ= 6 pC is conceivable for a 1000-μm^2 array of nanowires when these are infiltrated by

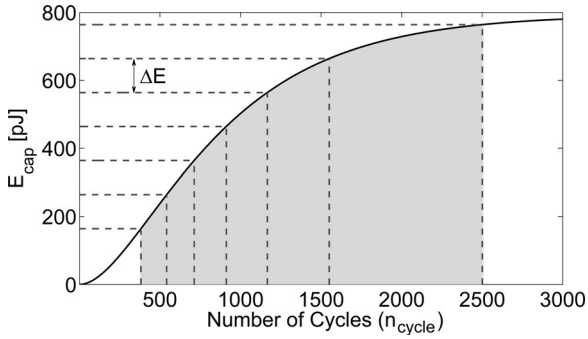

Fig. 3. Energy stored in the ultra-nanocapacitor as a function of the number of cycles.

insulating polymers. The capacitance of an ultra-nanocapacitor $C_{\rm cap}$ depends on the capacitor technology that is used and the capacitor size. Among others, a capacitance of $C_{\rm cap}$= 9 nF is conceivable for electrostatic ultra-nanocapacitors based on onion-like-carbon electrodes with the target size of nanosensor motes [25].

For these values, the energy capacity $E_{\rm cap-max}$ in (3) is approximately 800 pJ when the capacitor $C_{\rm cap}$ is charged at V_g= 0.42 V. Then, the number $n_{\rm cycle}$ of cycles (4) which are needed to charge the capacitor $C_{\rm cap}$ up to 95% of its energy capacity $E_{\rm cap-max}$ in (3) is approximately 2500 cycles. For example, for a constant vibration generated by the vents of the air conditioning system of an office (vibration frequency $1/t_{\rm cycle}$ = 50 Hz), the time needed to fully charge the capacitor $C_{\rm cap}$ up to its capacity $E_{\rm cap-max}$ is approximately $n_{\rm cycle}t_{\rm cycle}$= 50 s. For the human heart beat ($1/t_{\rm cycle}$ = 1 Hz), the recharging time is 42 min.

Finally, the energy stored in the capacitor $E_{\rm cap}$ is shown in Fig. 3 as a function of the number of cycles. For example, to increase the energy stored in the capacitor $E_{\rm cap}$ by a fixed amount ΔE= 100 pJ from an initial value of 164 pJ, the number $n_{\rm cycle}$ of needed cycles is approximately 160 cycles. To increase the stored energy in the capacitor $E_{\rm cap}$ by the same amount ΔQ=100 pJ but for the case in which this is already charged at $E_{\rm cap}$= 564 pJ, 384 cycles are needed. However, note that there is *no need to wait for the ultra-nanocapacitor to be fully recharged* to consume its energy.

These values are meaningful only when jointly analyzed with the energy consumption characteristics of nanosensor motes. Several processes affect the energy consumption of nanosensor motes (e.g., sensing, computing, data storing, and communication). Due to the fact that nanosensor motes are envisioned to operate at very high frequencies [1]–[3], communication is considered as the most energy demanding process. For this, we describe next the energy consumption due to communication in WNSNs.

III. Energy Consumption in Terahertz Band Communication

The communication options for nanosensor motes are very limited. The reduction of the antenna size in a classical sensor mote down to a few hundreds of nanometers would impose the use of very high operating frequencies (several hundreds of terahertz), thus limiting the feasibility of WNSNs. Alternatively, nanomaterials enable the development of nanoantennas that can operate at much lower frequencies. Ongoing research on the characterization of the EM properties of graphene, lately referred to as the *wonder material of the 21st century* [13], [41], points to the terahertz band (0.1–10.0 THz) as the frequency of novel nanoantennas [13], [27], [41] and nanotransceivers [17], [22], [24].

The terahertz band (0.1–10.0 THz) [9] is one of the least explored frequency ranges in the EM spectrum. In [10] and [14], we developed a new channel model for terahertz band communications and we showed how the absorption from several molecules in the medium attenuates and distorts the traveling waves and introduces additive colored Gaussian noise. Despite these phenomena, this band can theoretically support very large bit-rates, up to several hundreds of terabit/second, for distances below 1 m. In addition, having a very large bandwidth enables new simple communication mechanisms suited to the limited capabilities of nanodevices.

In this direction, we have recently proposed time-spread ON–OFF keying (TS-OOK), a new communication scheme based on the exchange of very short pulses spread in time [11]. For the time being, it is technologically not feasible to generate a high-power carrier signal in the terahertz band with a nanoscale transceiver. As a result, classical communication paradigms based on the transmission of continuous signals cannot be used. Alternatively, very short pulses can be generated and efficiently radiated from the nanoscale. In particular, femtosecond-long pulses, which have their main frequency components in the terahertz band, are already being used in several applications such as nanoscale imaging [35]. Note that this scheme clearly differs from impulse radio ultrawide-band systems [36], in which nanosecond-long pulses are transmitted by using time hopping orthogonal sequences with a pulse-position modulation.

In Fig. 4, we show an example of TS-OOK for the case in which two nanosensor motes are simultaneously transmitting different binary sequences to a third nanosensor mote. The upper plot corresponds to the transmission of the sequence "1100" by the first nanosensor mote. A logical "1" is represented by a short pulse with duration T_p and a logical "0" is represented by silence. The time T_s between symbols is much larger than the symbol duration T_p. The transmitted signal is propagated through the channel and corrupted with noise. Similarly, the second plot shows the sequence transmitted by the second nanosensor mote, "1001." Finally, the signal at the receiver is shown in the third subplot. Note that the receiver can decode the two sequences independently and without collisions, provided that the symbols of the first and the second motes do not exactly overlap in time. Moreover, there are no collisions between "0"s, and collisions between "0"s and "1"s are only harmful from the "0"s perspective. This scheme requires tight symbol synchronization between transmitting and receiving nanodevices, which can be achieved by means of a new nanotransceiver architecture [4].

For our analysis, we are interested in quantifying the energy consumed in the transmission and in the reception of a packet, $E_{\rm packet-tx}$ and $E_{\rm packet-rx}$, respectively. We consider

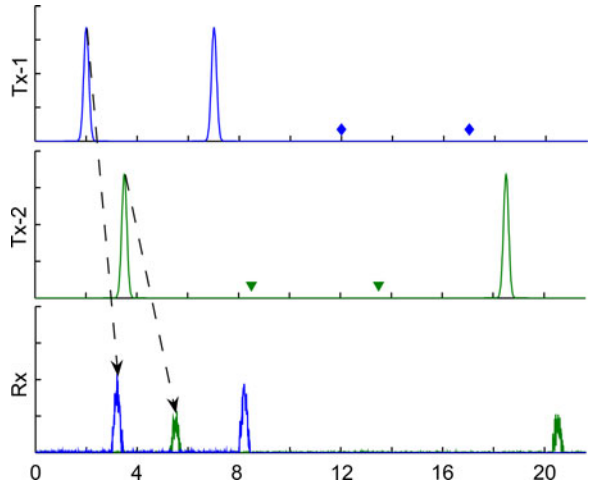

Fig. 4. TS-OOK illustration: (top) first mote transmitting the sequence "1100"; (middle) second mote transmitting the sequence "1001"; (bottom) overlapped sequences at the receiver side.

that a packet consists of N_{bits} bits, from which N_{header} bits correspond to the header and N_{data} corresponds to the payload of the packet. Then, the energy consumed when transmitting or receiving a packet is given by

$$E_{\text{packet}-tx} = N_{\text{bits}} W E_{\text{pulse}-tx}$$
$$E_{\text{packet}-rx} = N_{\text{bits}} E_{\text{pulse}-rx} \quad (6)$$

where $E_{\text{pulse}-tx}$ and $E_{\text{pulse}-rx}$ are the energy consumed in the transmission and in the reception of a pulse, respectively, and W refers to the coding weight, i.e., the probability of transmitting a pulse ("1") instead of being silent ("0"). On average, the number of "1"s and "0"s in a packet is balanced, i.e., W= 0.5 [12]. Note that by being silent, the transmitter can reduce its energy consumption, but the receiver still consumes the same amount of energy to detect the symbol.

Finally, we need to determine realistic values for $E_{\text{pulse}-tx}$ and $E_{\text{pulse}-rx}$. Based on the numerical results provided in [11], we fix the energy per pulse to $E_{\text{pulse}-tx}$= 1 pJ and target transmission distances in the order of 10 mm. We also consider that the energy consumed in the reception of a pulse $E_{\text{pulse}-rx}$ is approximately 10 times lower than $E_{\text{pulse}--tx}$, which is a valid assumption for ultralow power transceivers [20]. With these numbers, the energy consumption $E_{\text{packet}--tx}$ for the transmission of, for example, a 200 bit-long packet is 200 pJ. Thus, given an energy capacity $E_{\text{cap}-\max}$ in (3) of 800 pJ, only four packets can be transmitted with a fully charged ultra-nanocapacitor. From this result, it is clear that the energy harvesting process and the energy consumption process are not balanced. In order to capture the energy fluctuations of the energy in nanosensor motes, we need to jointly analyze the energy harvesting and the energy consumption processes. Moreover, the correlation between the energy in the nanodevices and the overall network traffic and multiuser interference needs to be captured.

IV. Model for the Available Energy of Nanosensor Motes

Classical energy models cannot be used for nanosensor motes mainly because they are focused on analyzing and minimizing the energy consumption of wireless devices whose total energy decreases until their batteries are depleted [31], [33]. Recently, a few models for energy harvesting sensors have been proposed in [16], [18], [21], and [30]. However, these models cannot be directly used in WNSNs because they do not capture the peculiarities of the energy harvesting and the energy consumption in nanosensors. In particular, the analysis in [18] is optimized for solar energy harvesting sensor networks, in which the energy harvesting rate changes over time by following a realistic sunlight profile. It is also assumed that the battery of the sensors can store enough energy to operate for several hours. In WNSNs, sunlight may not be available in the envisioned applications and, in addition, the energy capacity of the battery is expectedly very small. In [16], [21], and [30], the energy harvesting rate is considered constant, which is not a valid assumption for WNSNs as we discussed in Section II. Moreover, the impact of the energy fluctuations on the network traffic and behavior is not analyzed. Experimental results are given in [8], [19], and [42], but no analytical solution is provided. As we mentioned before, nanosensor motes have not been built yet, and developing an analytical energy model is necessary to first identify and understand the capabilities and limitations of WNSNs and ultimately aid in the design of future WNSN protocols and network architectures.

In this section, we develop an energy model for nanosensor motes based on the energy harvesting process described in Section II and the communication energy consumption process described in Section III. This proposed model successfully captures the overall network behavior by taking into account the changes over time in the total network traffic and the multiuser interference. From the steady-state analysis of the model, a mathematical framework is set to further investigate the impact on the network performance of different communication parameters. The major outcome of this model is the energy probability distribution of a nanosensor as a function of the energy harvesting and the communication parameters.

A. Nanosensor Energy Model Definition

We model the nanosensor mote energy by means of a *nonstationary continuous-time Markov process*, $\mathcal{E}(t)$, which describes the evolution in time t of the energy states of a nanosensor mote. As described in Section II, the energy harvesting process follows a Poisson distribution when ambient vibrations are considered. For the communication process, we consider that nanosensors generate new information also by following a Poisson distribution. Due to the fact that packets might not be always successfully transmitted or received, retransmissions are allowed. By limiting the number of retransmissions per packet and by exponentially randomizing the time between transmissions, the network traffic can be characterized by a *time-varying Poisson distribution*. Thus, the nanosensor mote energy can be modeled with a Markov process.

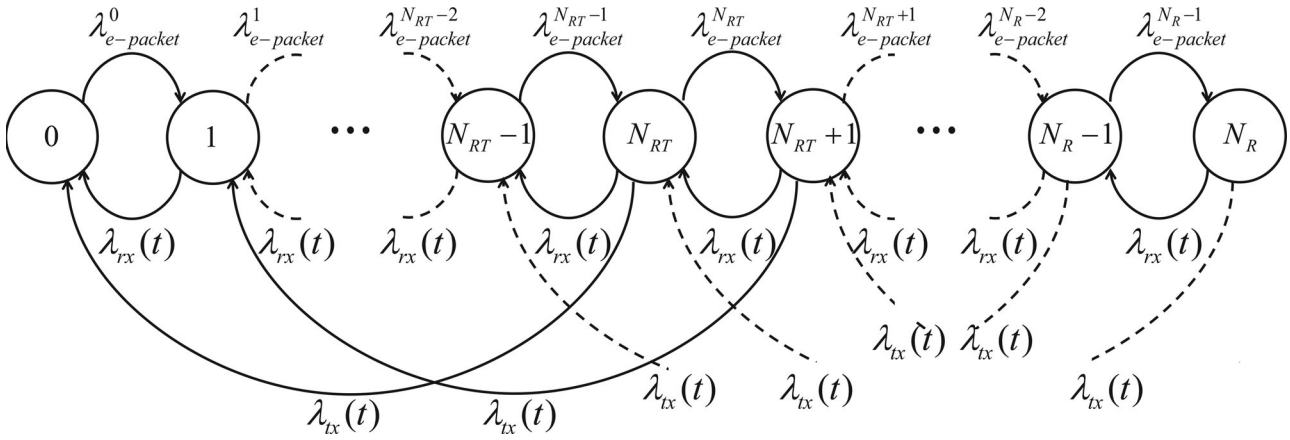

Fig. 5. Markov chain representation of the proposed model for the temporal energy variations in nanosensors.

The process $\mathcal{E}(t)$ is represented by the Markov chain in Fig. 5 and it is fully characterized by its transition rate matrix $\boldsymbol{Q}(t)$ in (7). Each element in the matrix $q^{ij}(t)$ refers to the rate at which the transitions from state i to state j occur, and $q^{ii}(t) = -q^{i}(t) = -\sum_{j\neq i} q^{ij}(t)$, where q^i refers to the lifetime of the state i. We define the state probability vector as $\boldsymbol{\pi}(t) = \{\pi^0(t), \pi^1(t), \ldots\}$, where $\pi^n(t)$ refers to the probability of finding the process $\mathcal{E}(t)$ in state n at time t. In (7), shown at the bottom of the page, we describe the model in detail.

1) Energy States: Each state in the Markov chain in Fig. 5 corresponds to an energy state of the nanosensor. In the state $n = 0$, the nanosensor only has a minimal energy $E_{\min}$ necessary to operate. In the state $n = 1$, the nanosensor has energy $E_{\text{packet}-rx}$ to receive one packet, as defined in (6). In general, the energy E^n of the state n is

$$E^n = E_{\min} + nE_{\text{packet}-rx}. \tag{8}$$

In the maximum energy state, which is given by $n = N_R$, the capacitor is full, which corresponds to having enough energy either to transmit N_T information packets or to receive N_R packets. The values of N_T and N_R are given by

$$N_T = \left\lfloor \frac{E_{\text{cap}-\max} - E_{\min}}{E_{\text{packet}-tx}} \right\rfloor$$
$$N_R = \left\lfloor \frac{E_{\text{cap}-\max} - E_{\min}}{E_{\text{packet}-rx}} \right\rfloor \tag{9}$$

where $E_{\text{cap}-\max}$ refers to the energy capacity of the harvesting system given by (3), and $E_{\text{packet}-tx}$ and $E_{\text{packet}-rx}$ are the energy consumed in the transmission and in the reception of an N_{bits} long packet, respectively, defined in (6). The operator $\lfloor\cdot\rfloor$ returns the highest integer number that is lower than the operand. For this model, $N_R > N_T$, and the total number of states corresponds to $N_R + 1$. For convenience, we define $N_{RT} = N_R/N_T$ as the number of packets received with the energy required for the transmission of a packet.

2) Packet Energy Harvesting Rate: As shown in Fig. 5, the transition from an energy state n to a state $n+1$ happens according to the packet energy harvesting rate $\lambda^n_{e\text{-packet}}$. As described in Section II, due to the nonlinearities in the energy harvesting process, the energy harvesting rate λ_e in (5) depends on the current energy state n. As a result, the transitions between states are not homogenous, but differ for every state.

The energy rate $\lambda^n_{e\text{-packet}}$ in energy-packet/second between an energy state n and an energy state $n+1$ can be written as a function of the energy in the current state E^n and the energy required to receive a packet $E_{\text{packet}-rx}$:

$$\lambda^n_{e\text{-packet}} = \frac{\lambda_e\left(E^n, E_{\text{packet}-rx}\right)}{E_{\text{packet}-rx}} \tag{10}$$

where λ_e is the energy harvesting rate in Joule/second in (5).

3) Packet Transmission and Reception Rates: As shown in Fig. 5, the transition from a higher energy state to a lower energy

$$\boldsymbol{Q} = \begin{array}{c} \\ 0 \\ 1 \\ 2 \\ \vdots \\ N_{RT}-1 \\ N_{RT} \\ N_{RT}+1 \\ \vdots \\ N_R \end{array}\!\!\begin{array}{c} \begin{array}{cccccccc} 0 & 1 & 2 & \cdots & N_{RT}-1 & N_{RT} & N_{RT}+1 & \cdots & N_R \end{array} \\ \begin{pmatrix} -\lambda^0_e & \lambda^0_e & 0 & \cdots & 0 & 0 & 0 & \cdots & 0 \\ \lambda_{rx}(t) & -\left(\lambda^1_e + \lambda_{rx}(t)\right) & \lambda^1_e & \cdots & 0 & 0 & 0 & \cdots & 0 \\ 0 & \lambda_{rx}(t) & -\left(\lambda^2_e + \lambda_{rx}(t)\right) & \cdots & 0 & 0 & 0 & \cdots & 0 \\ \vdots & \vdots & \vdots & \ddots & \vdots & \vdots & \vdots & \ddots & \vdots \\ \lambda_{tx}(t) & 0 & 0 & \cdots & \lambda_{rx}(t) & -\left(\lambda^{N_{RT}}_e + \lambda_{rx}(t) + \lambda_{tx}(t)\right) & \lambda^{N_{RT}}_e & \cdots & 0 \\ \vdots & \vdots & \vdots & \ddots & \vdots & \vdots & \vdots & \ddots & \vdots \\ 0 & 0 & 0 & \cdots & 0 & 0 & 0 & \cdots & -(\lambda_{rx}(t) + \lambda_{tx}(t)) \end{pmatrix} \end{array} \tag{7}$$

state is governed by the packet transmission rate $\lambda_{tx}(t)$ and the packet reception rate $\lambda_{rx}(t)$. The transmission of a packet results in a transition between a state n and a state $n - N_{RT}$. The reception of a packet results in a transition between a state n and the state $n-1$. $\lambda_{tx}(t)$ and $\lambda_{rx}(t)$ depend on the packet generation rate λ_{packet} of a nanosensor, which we consider constant, the relayed traffic λ_{neigh} and the energy states of all the nanosensors involved in the communication process (transmitter, receiver, and interfering nodes). The overall network traffic and the energy in the nanodevices are correlated and their relation needs to be captured.

To determine $\lambda_{tx}(t)$ and $\lambda_{rx}(t)$ we can proceed as follows. First, in order to successfully transmit a packet, the following conditions need to be satisfied:

1) A packet cannot be transmitted if the energy level of the transmitting nanosensor, modeled by the process $\mathcal{E}_{tx}(t)$, at transmission time t_0 is lower than N_{RT}, i.e., $\mathcal{E}_{tx}(t_0) \in \{0, 1, \ldots, N_{RT}-1\}$. This probability can be written as

$$p_{\text{drop}-tx}(t) = \sum_{i=0}^{N_{RT}-1} \pi_{tx}^{i}(t) \tag{11}$$

where $\pi_{tx}^{i}(t)$ is an element of the vector $\boldsymbol{\pi}_{tx}(t) = \left\{\pi_{tx}^{0}(t), \pi_{tx}^{1}(t), \ldots\right\}$, which is the state probability vector of the process $\mathcal{E}_{tx}(t)$.

2) A packet will not be received if the energy state of the receiving nanosensor, modeled by the process $\mathcal{E}_{rx}(t)$, at time $t_0 + T_{\text{prop}}$ is $n = 0$, where T_{prop} refers to the propagation delay between the transmitter and the receiver. This probability is given by

$$p_{\text{drop}-rx}(t) = \pi_{rx}^{0}(t) \tag{12}$$

where $\pi_{rx}^{0}(t)$ is an element of the vector $\boldsymbol{\pi}_{rx}(t) = \left\{\pi_{rx}^{0}(t), \pi_{rx}^{1}(t), \ldots\right\}$, which is the state probability vector of the process $\mathcal{E}_{rx}(t)$.

3) A packet will not be properly received if the channel introduces transmission errors. This probability is

$$p_{\text{error}} = 1 - (1 - \text{BER})^{N_{\text{bits}}} \tag{13}$$

where BER refers to the bit error rate and N_{bits} is the packet length in bits, defined as in Section III.

4) A packet will not be properly received if it collides with other nanosensors' transmissions. This probability can be written as

$$p_{\text{coll}}(t) = 1 - e^{-\lambda_{\text{net}}(t) W T_p N_{\text{bits}}} \tag{14}$$

where $\lambda_{\text{net}}(t)$ refers to the network traffic, W is the coding weight, T_p is the pulse duration, and N_{bits} is the packet length. This probability is in general much lower than $p_{\text{drop}-tx}(t)$ and $p_{\text{drop}-rx}(t)$ due to the fact that the transmission of the information with very short pulses minimizes the chances of having a collision. Note that, as described in Section III, the packets only collide if their symbols exactly overlap in time and silences (logical "0"s) do not create collisions.

Based on these, we define the probability $p_{\text{success}}(t)$ of successful transmission at time t as

$$\begin{aligned} p_{\text{success}}(t) = &\left(1 - p_{\text{drop}-tx}(t)\right)\left(1 - p_{\text{drop}-rx}(t)\right) \\ &\cdot \left(1 - p_{\text{error}}\right)\left(1 - p_{\text{coll}}(t)\right). \end{aligned} \tag{15}$$

Then, the total traffic rate $\lambda_{\text{net}}(t)$ between two neighboring nanosensors in (14) is given by

$$\begin{aligned} \lambda_{\text{net}}(t) &= \sum_{i=0}^{K} \left(\lambda_{\text{packet}} + \lambda_{\text{neigh}}\right) \\ &\quad \cdot \left(1 - p_{\text{drop}-tx}(t)\right)\left(1 - p_{\text{success}}(t)\right)^{i} = \\ &= (M+1)\,\lambda_{\text{packet}}\left(1 - p_{\text{drop}-tx}(t)\right) \\ &\quad \cdot \frac{1 - \left(1 - p_{\text{success}}(t)\right)^{K+1}}{p_{\text{success}}(t)} \end{aligned} \tag{16}$$

where K is the maximum number of retransmissions, λ_{packet} refers to the packet generation rate and λ_{neigh} refers to the rate of the traffic coming from the neighbors, which we consider to be equal to $M\lambda_{\text{packet}}$, where M is the number of neighbors. In this definition, we take into account that only if the transmitter has enough energy, an attempt to transmit will result in a packet in the channel.

Then, the reception rate $\lambda_{rx}(t)$ is given by

$$\lambda_{rx}(t) = \lambda_{\text{net}}\left(1 - p_{\text{drop}-rx}(t)\right) \tag{17}$$

where it is taken into account that only packets that are not dropped in reception are counted by the receiver. Note that even if the packet is not properly received due to channel errors or collisions, the energy is consumed.

Finally, the transmission rate $\lambda_{tx}(t)$ is given by

$$\lambda_{tx}(t) = \lambda_{\text{packet}} \frac{1 - \left(1 - p_{\text{success}}(t)\right)^{K+1}}{p_{\text{success}}(t)} \tag{18}$$

where we are taking into account that a nanosensor attempts to transmit the packets that it generates and all the packets that it has received without errors and which have not collided.

Up to this point, we have defined all the terms in the model for the available energy of nanosensors.

B. Nanosensor Mote Energy in the Steady State

In classical sensor networks, a usual metric to measure the energy efficiency of a communication solution is the network lifetime, i.e., the time between the moment at which the network starts functioning until the time at which the first sensor depletes its battery. In self-powered networks, the network lifetime tends to infinite, given that even if at some point a nanosensor runs out of energy, there is a certain probability that it will recharge itself.

We are interested in determining the behavior of the system in the steady state. For this, we assume that the network reaches an equilibrium when time tends to infinity. This is correct if we consider the energy harvesting rate λ_e and the packet generation rate λ_{packet} to be stationary. Then, in the steady state, the state probability vector $\boldsymbol{\pi}$, the transition rate matrix $\boldsymbol{Q}$ given by (7),

and (11), (12), (14), (15), (16), (17), and (18) lose their temporal dependence. In addition, if we consider the source of vibration and the traffic in the network to be homogenous, the steady state is the same for all the nanodevices. Therefore, the state probability vectors $\boldsymbol{\pi}_{tx}$ in (11) and $\boldsymbol{\pi}_{rx}$ in (12) can be replaced by $\boldsymbol{\pi}$.

In this case, the probability mass function (p.m.f.) of the nanosensor mote energy can be written as a function of the steady state probability vector $\boldsymbol{\pi}$:

$$p_{\mathcal{E}}\left(E^i\right) = \pi^i \tag{19}$$

i.e., the probability of having an energy exactly equal to $E^i = E_{\min} + iE_{\text{packet}-rx}$ is π^i. Similarly, the cumulative distribution function (c.d.f.) of the nanosensor mote energy is

$$F_{\mathcal{E}}\left(E\right) = \sum_i \left\{\pi^i | E_i \leq E\right\} \tag{20}$$

and the probability of a nanosensor to have at least E energy is given by $1 - F_{\mathcal{E}}\left(E\right)$.

To determine the steady state probabilities in (19) and (20), we need to solve the system of $N_R + 1$ equations given by $\boldsymbol{\pi}Q = \mathbf{0}$ with the additional equation given by the normalization condition for the steady state probability vector, $\sum_i \pi^i = 1$. Note the transition rate matrix $\boldsymbol{Q}$ in (7) depends on the packet transmission rate λ_{tx} from (18) and the packet reception rate λ_{rx} from (17), which depend on the total traffic λ_{net} in (16). This depends on the probabilities of dropping a packet in transmission or in reception, $p_{\text{drop}-tx}$ in (11) and $p_{\text{drop}-rx}$ in (12), respectively, the probability of having channel errors, p_{error} in (13), and the probability of having a collision p_{coll} in (14). On their turn, these probabilities depend on the steady state probabilities of the system $\boldsymbol{\pi}$. Therefore, (18), (17), (16), (11), (12), (13), and (14) need to be jointly solved with the steady state conditions for $\boldsymbol{\pi}$ and $\boldsymbol{Q}$. These form a system of $N_R + 10$ equations from which finding a closed-form expression of $\boldsymbol{\pi}$ is not feasible. However, these equations define a mathematical framework that allows us to numerically investigate the effect of different system parameters on the network performance.

V. Performance of Perpetual WNSNs

In this section, first, we validate the analytical energy model introduced in Section IV by means of simulation. Then, we use this model to investigate the impact of energy on three different common metrics in WNSNs.

A. Validation of the Nanosensor Energy Model

We use MATLAB to simulate a WNSN composed by 100 nodes, which are uniformly distributed over a 1 cm^2 surface and which transmit information in a multi-hop fashion [1]. Each nanosensor mote harvests vibrational energy by means of a piezoelectric nanogenerator (see Section II) with the following parameters. The energy capacity $E_{\text{cap}-\max}$ in (3) is 800 pJ, which corresponds to the energy in a capacitor with C_{cap}= 9 nF charged at V_g= 0.42 V. For the computation of the energy rate λ_e in (5), an ambient vibration with an average time between vibrations t_{cycle} = 1/50 s is considered. The amount of charge ΔQ harvested per cycle is 6 pC. The battery is fully discharged at the beginning of a simulation.

Each nanosensor mote generates new packets by following a Poisson distribution with parameter $\lambda_{\text{packet}} = \lambda_{\text{info}}/N_{\text{bits}}$, where λ_{info} accounts for both new data and forwarded traffic, and N_{bits} is the packet length. A packet is composed by N_{header}= 32 bits of header and N_{data}= 96 bits for the payload. Packets are broadcasted to the neighboring nodes by means of TS-OOK (see Section III). The length of the pulses considered in this scheme is of 100 femtosecond. The separation between symbols (pulses or silences) is of 100 ps. The energy consumption for the transmission of a pulse $E_{\text{pulse}-tx}$ and for the reception of a pulse $E_{\text{pulse}-rx}$ are 1 pJ and 0.1 pJ, respectively (this provides the system with a BER of 10^{-4} at 10 mm [11]). The energy consumption in the transmission and in the reception of a packet, $E_{\text{packet}-tx}$ and $E_{\text{packet}-rx}$, respectively, are computed from (6) (coding weight $W = 0.5$).

To validate our model in Section IV, we compare the normalized histogram of the nanosensors energy evolution over time in the simulations with the p.m.f. of the nanosensor mote energy, $p_{\mathcal{E}}$ in (19), obtained from the proposed analytical model. A total of twenty 10 000-s long simulations are used to compute the histogram. The initial samples of each run are discarded to account only for the steady state of the network. This is shown in Fig. 6 for different packet generation rates, λ_{info}. The simulation results and the numerical results from the steady state analysis of the energy model match accurately. From the figures, it is clear that for low packet generation rates, e.g., 3 bit/s, the p.m.f. is centered around the highest energy levels, i.e., the device has enough energy for the majority of the cases. As the information generation rate is increased, the p.m.f. of the nanosensor mote energy shifts toward the lower energy levels. In light of these results, we next analyze the performance of energy harvesting WNSN by means of our analytical model.

B. End-to-End Successful Packet Delivery Probability

The first WNSN performance metric that we investigate is the end-to-end successful packet delivery probability. This is defined as

$$p_{\text{success}-\text{e2e}} = \left(1 - \left(1 - p_{\text{success}}\right)^{K+1}\right)^{N_{\text{hop}}} \tag{21}$$

where N_{hop} is the total number of hops, K is the total number of retransmissions and p_{success} refers to the probability of successful transmission in (15). In our analysis, we consider that the average distance between two nanosensors is constant and, thus, the average number of hops N_{hop} for a packet is fixed for a given end-to-end transmission distance. In our analysis, we consider an average of 5 hops per packet.

In Fig. 7, the end-to-end successful packet delivery probability $p_{\text{success}-\text{e2e}}$ is shown as a function of the packet size N_{bits} and the number of retransmissions K. From this representation, it is clear that there is an optimal packet size and number of retransmissions that maximize the $p_{\text{success}-\text{e2e}}$. On the one hand, the transmission of shorter packets increases the number of energy states N_R from (9) in which a nanosensor can be. This increases the number of packets that can be processed in a single

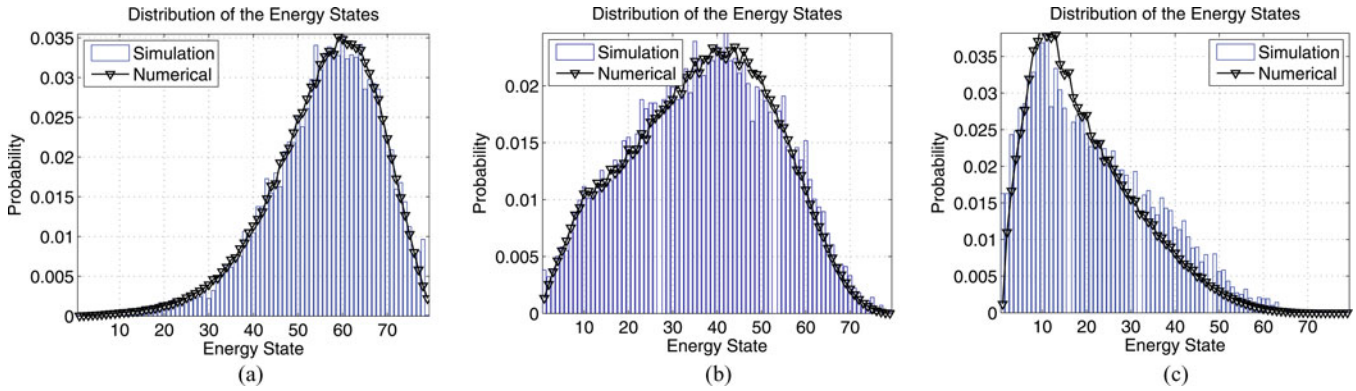

Fig. 6. Probability mass function $f_{\mathcal{E}}\left(E^i\right)$ of the nanosensor mote energy in (19) as a function of the energy state i for different information generation rates (N_{bits}= 96 bits, K = 5). (a) $\lambda_{\text{info}} = 3$ bit/s. (b) $\lambda_{\text{info}} = 5$ bit/s. (c) $\lambda_{\text{info}} = 7$ bit/s.

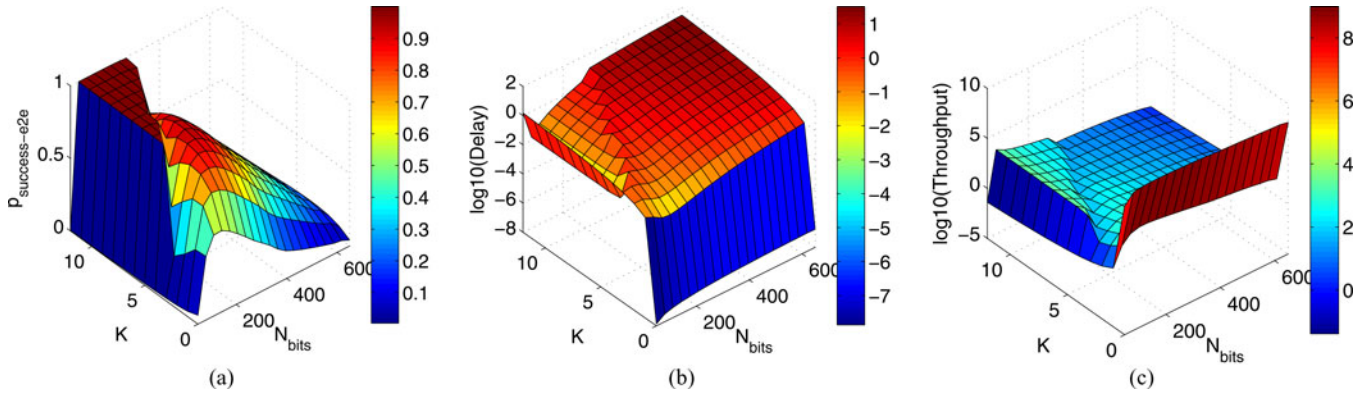

Fig. 7. End-to-end successful packet delivery probability (21), end-to-end packet delay (23) and throughput (26) as functions of N_{bits} and K (λ_{info}= 5 bits, N_{hops}=5). (a) $p_{\text{success-e2e}}$. (b) T_{e2e}. (c) th_{put}.

energy charge. In addition, the packet energy harvesting rate λ_e^n in (10) increases by decreasing the packet size. Moreover, due to the nonlinearities in the energy harvesting process, the rate at which the energy is harvested is higher when the nanodevice is approaching its lower energy states (see Fig. 3). Therefore, the time needed to recover from the lower energy level is shorter. On the other hand, for a constant information generation rate λ_{info}, a higher number of packets $\lambda_{\text{packet}} = \lambda_{\text{info}}/N_{\text{data}}$ needs to be transmitted to convey the same amount of information. This can have a major impact in the network traffic λ_{net} in (16) as well as in the energy of a relaying node. In addition, each packet has a fixed header with N_{header} bits. The optimal scheme corresponds to transmit 48 bit packets with up to 1 retransmission.

C. End-to-End Packet Delay

The second metric in our analysis is the end-to-end packet delay T_{e2e}, which is given by

$$T_{\text{e2e}} = N_{\text{hop}} \sum_{i=0}^{K} \left(T_{\text{prop}} + T_{\text{data}} + iT_{\text{t/o}}\right) \tag{22}$$

where N_{hop} is the total number of hops and K is the total number of retransmissions. T_{prop} is the propagation time, T_{data} is the packet transmission time, and $T_{\text{t/o}}$ is a time-out time, which we define as follows:

$$T_{\text{t/o}} = p_{\text{drop}-tx} T_{RT} + (1 - p_{\text{drop}-tx}) \left(p_{\text{drop}-rx} T_R + (1 - p_{\text{drop}-rx}) (1 - p_{\text{error}} p_{\text{coll}}) T_o\right) \tag{23}$$

where $p_{\text{drop-}tx}$ stands for the probability of having enough energy to transmit the packet (11), $p_{\text{drop}-rx}$ refers to the probability of having enough energy to receive a packet (12). p_{error} and p_{coll} are the probabilities of having channel errors or suffering collisions, respectively, and are given by (13) and (14), respectively. T_{RT} refers to the average time needed to harvest enough energy to transmit a packet, and it is given by:

$$T_{RT} = \sum_{i=0}^{N_{RT}-1} \pi_{tx}^i / q_{tx}^i \tag{24}$$

where N_{RT} is the number of packets that can be received with the energy required for the transmission of a packet, π_{tx}^i refers to the probability of finding the process $\mathcal{E}_{tx}$ in state i, and q_{tx}^i is the ith element in the diagonal of the transition rate matrix $\boldsymbol{Q}_{tx}$. T_R stands for the average time needed to harvest enough energy to receive a packet, and it is given by

$$T_R = 1/q_{rx}^0 \tag{25}$$

where q_{rx}^0 refers to the first element of the transition rate matrix $\boldsymbol{Q}_{rx}$ of the receiver. We consider in our analysis that a

nanosensor will attempt to retransmit the packet after waiting a back-off time proportional to T_R. Finally, T_o is a random back-off time before retransmitting when channel errors or collisions are the reason for nonproper reception of a packet.

The end-to-end packet delay is shown in Fig. 7 as a function of the packet size N_{bits} and the number of retransmissions K. From this representation, it is clear that there is an optimal packet size and number of retransmissions that minimize the T_{e2e}. In addition to the previous reasoning regarding the packet length, note that the number of retransmissions has also a major impact on the network performance. By increasing the number of retransmissions K, the probability of successful transmission p_{success} and the end-to-end delay are increased. However, if the reason to retransmit is the lack of energy either at the transmitter or the receiver side, the necessary waiting time $T_{\text{t/o}}$ to recharge the energy system up to a minimal level will determine the end-to-end delay T_{e2e} from (23). Intuitively, a packet that can be transmitted without having to wait in any nanosensor can reach the destination at speeds that approach the capacity of the channel (tens of gigabits/second for the transmission power in this scenario). On the contrary, if the packet needs to wait several times for a nanosensor to recharge, the end-to-end delay will approach the energy harvesting rate, which is several orders of magnitude lower than the information rate. In this case, the optimal strategy would be to transmit 48-bit long packets without retransmissions.

D. Throughput

The third metric that we consider is the WNSN throughput, th_{put}, which is defined as

$$\text{th}_{\text{put}} = \frac{N_{\text{data}} p_{\text{success-e2e}}}{T_{\text{e2e}}} \tag{26}$$

where N_{data} refers to the number of data bits per packet, $p_{\text{success-e2e}}$ refers to the end-to-end successful packet delivery probability in (21) and T_{e2e} is the end-to-end packet delay from (23). The throughput is shown in Fig. 7 as a function of the packet size N_{bits} and the number of retransmissions K. Similarly than before, there is an optimal packet size that maximizes the network throughput. The optimal parameters for this network are N_{bits}=175 bits without retransmissions.

VI. Conclusion

WNSNs will boost the applications of nanotechnology in many fields of our society, ranging from healthcare to homeland security and environmental protection. One of the major bottlenecks in WNSNs is posed by the very limited energy that can be stored in the nanosensors in contrast to the energy requirements of the communication techniques envisioned for this new networking paradigm.

In this paper, we proposed the first energy model for self-powered nanosensor motes with the final goal of jointly analyzing the energy harvesting and the energy consumption processes. For this, we developed an analytical model for the energy harvesting process of a nanosensor mote powered by a piezoelectric nanogenerator, we reviewed the energy consumption process due to communication among nanosensors in the terahertz band, and we modeled the temporal variations in the nanosensor energy and their correlation with the overall network traffic. From this model, we developed a mathematical framework to investigate the impact of the packet size and the retransmission policy on the end-to-end successful packet delivery probability, the end-to-end packet delay, and the throughput of WNSNs. Integrated nanosensor motes have not been built yet and, thus, the development of an analytical energy model is a fundamental step towards the design of WNSNs architectures and protocols.

References

[1] I. F. Akyildiz and J. M. Jornet, "Electromagnetic wireless nanosensor networks," *Nano Commun. Netw.*, vol. 1, no. 1, pp. 3–19, Mar. 2010.

[2] I. F. Akyildiz and J. M. Jornet, "The internet of nano-things," *IEEE Wireless Commun. Mag.*, vol. 17, no. 6, pp. 58–63, Dec. 2010.

[3] I. F. Akyildiz, J. M. Jornet, and M. Pierobon, "Nanonetworks: A new frontier in communications," *Commun. ACM*, vol. 54, no. 11, pp. 84–89, Nov. 2011.

[4] R. G. Cid-Fuentes, J. M. Jornet, E. Alarcon, and I. F. Akyildiz, "A nano-transceiver architecture for pulse-based communications in the terahertz band," in *Proc. IEEE Int. Conf. Commun.*, Jun. 2012, pp. 1–6.

[5] F. Cottone, H. Vocca, and L. Gammaitoni, "Nonlinear energy harvesting," *Phys. Rev. Lett.*, vol. 102, no. 8, pp. 080601-1–080601-4, Feb. 2009.

[6] L. Gammaitoni, I. Neri, and H. Vocca, "Nonlinear oscillators for vibration energy harvesting," *Appl. Phys. Lett.*, vol. 94, pp. 164102-1–164102-3, Apr. 2009.

[7] Y. Gao and Z. L. Wang, "Electrostatic potential in a bent piezoelectric nanowire. The fundamental theory of nanogenerator and nanopiezotronics," *Nano Lett.*, vol. 7, no. 8, pp. 2499–2505, 2007.

[8] J. Gummeson, S. S. Clark, K. Fu, and D. Ganesan, "On the limits of effective hybrid micro-energy harvesting on mobile CRFID sensors," in *Proc. 8th ACM Int. Conf. Mobile Syst., Appl., Serv.*, 2010, p. 14.

[9] IEEE 802.15 Wireless Personal Area Networks-Terahertz Interest Group (IGthz). [Online]. Available: http://www.ieee802.org/15/pub/IGthz.html.

[10] J. M. Jornet and I. F. Akyildiz, "Channel capacity of electromagnetic nanonetworks in the terahertz band," in *Proc. IEEE Int. Conf. Commun.*, May, 2010, pp. 1–6.

[11] J. M. Jornet and I. F. Akyildiz, "Information capacity of pulse-based wireless nanosensor networks," in *Proc. 8th Annu. IEEE Commun. Soc. Conf. Sens., Mesh Ad Hoc Commun. Netw.*, Jun. 2011, pp. 80–88.

[12] J. M. Jornet and I. F. Akyildiz, "Low-weight channel coding for interference mitigation in electromagnetic nanonetworks in the terahertz band," in *Proc. IEEE Int. Conf. Commun.*, Jun. 2011, pp. 1–6.

[13] J. M. Jornet and I. F. Akyildiz, "Graphene-based nano-antennas for electromagnetic nanocommunications in the terahertz band," in *Proc. 4th Eur. Conf. Antennas Propag.*, Apr. 2010, pp. 1–5.

[14] J. M. Jornet and I. F. Akyildiz, "Channel modeling and capacity analysis of electromagnetic wireless nanonetworks in the terahertz band," *IEEE Trans. Wireless Commun.*, vol. 10, no. 10, pp. 3211–3221, Oct. 2011.

[15] P. V. Kamat, "Harvesting photons with carbon nanotubes," *Nano Today*, vol. 1, no. 4, pp. 20–27, 2006.

[16] J. Lei, R. Yates, and L. Greenstein, "A generic model for optimizing single-hop transmission policy of replenishable sensors," *IEEE Trans. Wireless Commun.*, vol. 8, no. 2, pp. 547–551, Feb. 2009.

[17] Y. M. Lin, C. Dimitrakopoulos, K. A. Jenkins, D. B. Farmer, H. Y. Chiu, A. Grill, and P. Avouris, "100-GHz Transistors from wafer-scale epitaxial graphene," *Science*, vol. 327, no. 5966, Feb. 2010.

[18] R.-S. Liu, K.-W. Fan, Z. Zheng, and P. Sinha, "Perpetual and fair data collection for environmental energy harvesting sensor networks," *IEEE/ACM Trans. Network.*, vol. 19, no. 4, pp. 947–960, Aug. 2011.

[19] A. W. Maria Gorlatova and G. Zussman, "Networking low-power energy harvesting devices: Measurements and algorithms," presented at the Int. Conf. Comput. Commun., INFOCOM, Shanghai, China, Apr. 2011.

[20] S. J. Marinkovic and E. M. Popovici, "Nano-power wake-up radio circuit for wireless body area networks," in *Proc. IEEE Top. Conf. Biomed. Wireless Technol., Netw., Sens. Syst.*, Jan. 2011, pp. 398–401.

[21] B. Medepally, N. Mehta, and C. Murthy, "Implications of energy profile and storage on energy harvesting sensor link performance," in *Proc. IEEE Global Telecommun. Conf.*, 2009.

[22] J. Moon, D. Curtis, D. Zehnder, S. Kim, D. Gaskill, G. Jernigan, R. Myers-Ward, C. Eddy, P. Campbell, K.-M. Lee, and P. Asbeck, "Low-phase-noise graphene fets in ambipolar RF applications," *IEEE Electron Device Lett.*, vol. 32, no. 3, pp. 270–272, Mar. 2011.
[23] D. Niyato, E. Hossain, M. Rashid, and V. Bhargava, "Wireless sensor networks with energy harvesting technologies: A game-theoretic approach to optimal energy management," *IEEE Wireless Commun.*, vol. 14, no. 4, pp. 90–96, Aug. 2007.
[24] T. Palacios, A. Hsu, and H. Wang, "Applications of graphene devices in RF communications," *IEEE Commun. Mag.*, vol. 48, no. 6, pp. 122–128, Jun. 2010.
[25] D. Pech, M. Brunet, H. Durou, P. Huang, V. Mochalin, Y. Gogotsi, P. Taberna, and P. Simon, "Ultrahigh-power micrometre-sized supercapacitors based on onion-like carbon," *Nature Nanotechnol.*, vol. 5, no. 9, pp. 651–655, Sep. 2010.
[26] J. Riu, A. Maroto, and F. X. Rius, "Nanosensors in environmental analysis," *Talanta*, vol. 69, no. 2, pp. 288–301, 2006.
[27] M. Rosenau da Costa, O. V. Kibis, and M. E. Portnoi, "Carbon nanotubes as a basis for terahertz emitters and detectors," *Microelectron. J.*, vol. 40, no. 4–5, pp. 776–778, Apr. 2009.
[28] S. Roundy, P. K. Wright, and J. M. Rabaey, *Energy Scavenging for Wireless Sensor Networks: With Special Focus on Vibrations*. Norwell, MA: Kluwer, 2004.
[29] F. Schedin, A. K. Geim, S. V. Morozov, E. W. Hill, P. Blake, M. I. Katsnelson, and K. S. Novoselov, "Detection of individual gas molecules adsorbed on graphene," *Nature Mater.*, vol. 6, pp. 652–655, 2007.
[30] V. Sharma, U. Mukherji, V. Joseph, and S. Gupta, "Optimal energy management policies for energy harvesting sensor nodes," *IEEE Trans. Wireless Commun.*, vol. 9, no. 4, pp. 1326–1336, Apr. 2010.
[31] E. Shih, S.-H. Cho, N. Ickes, R. Min, A. Sinha, A. Wang, and A. Chandrakasan, "Physical layer driven protocol and algorithm design for energy-efficient wireless sensor networks," in *Proc. ACM Int. Conf. Mobile Comput. Network.*, 2001, pp. 272–287.
[32] S. Sudevalayam and P. Kulkarni, "Energy harvesting sensor nodes: Survey and implications," *IEEE Commun. Surv. Tutorials*, vol. 13, no. 3, pp. 443–461, Third Quarter 2011.
[33] Y. Wang, M. Vuran, and S. Goddard, "Stochastic analysis of energy consumption in wireless sensor networks," in *Proc. 7th Annu. IEEE Commun. Soc. Conf. Sens. Mesh Ad Hoc Commun. Netw.*, Jun. 2010, pp. 1–9.
[34] Z. L. Wang, "Towards self-powered nanosystems: From nanogenerators to nanopiezotronics," *Adv. Funct. Mater.*, vol. 18, no. 22, pp. 3553–3567, 2008.
[35] D. Woolard, P. Zhao, C. Rutherglen, Z. Yu, P. Burke, S. Brueck, and A. Stintz, "Nanoscale imaging technology for thz-frequency transmission microscopy," *Int. J. High Speed Electron. Syst.*, vol. 18, no. 1, pp. 205–222, 2008.
[36] H. Xu and L. Yang, "Ultra-wideband technology: Yesterday, today, and tomorrow," in *Proc. IEEE Radio Wireless Symp.*, Jan. 2008, pp. 715–718.
[37] S. Xu, B. J. Hansen, and Z. L. Wang, "Piezoelectric-nanowire-enabled power source for driving wireless microelectronics," *Nature Commun.*, vol. 1, no. 7, pp. 1–5, Oct. 2010.
[38] S. Xu, Y. Qin, C. Xu, Y. Wei, R. Yang, and Z. L. Wang, "Self-powered nanowire devices," *Nature Nanotechnol.*, vol. 5, pp. 366–373, 2010.
[39] H.-Y. Yeh, M. V. Yates, W. Chen, and A. Mulchandani, "Real-time molecular methods to detect infectious viruses," *Seminars Cell Develop. Biol.*, vol. 20, no. 1, pp. 49–54, 2009.
[40] C. R. Yonzon, D. A. Stuart, X. Zhang, A. D. McFarland, C. L. Haynes, and R. P. V. Duyne, "Towards advanced chemical and biological nanosensors-an overview," *Talanta*, vol. 67, no. 3, pp. 438–448, 2005.
[41] G. Zhou, M. Yang, X. Xiao, and Y. Li, "Electronic transport in a quantum wire under external terahertz electromagnetic irradiation," *Phys. Rev. B*, vol. 68, no. 15, p. 155309, Oct. 2003.
[42] T. Zhu, Z. Zhong, Y. Gu, T. He, and Z.-L. Zhang, "Leakage-aware energy synchronization for wireless sensor networks," in *Proc. 7th ACM Int. Conf. Mobile Syst., Appl., Serv.*, 2009, pp. 319–332.

Josep Miquel Jornet (S'08) received the Engineering degree in telecommunication engineering in 2008 and the Master of Science degree in information and communication technologies from the School of Electrical Engineering, Universitat Politècnica de Catalunya, Barcelona, Spain. He is currently working toward the Ph.D. degree in the Broadband Wireless Networking Laboratory, School of Electrical and Computer Engineering, Georgia Institute of Technology, Atlanta, with a fellowship from and Fundación Caja Madrid.

From September 2007 to December 2008, he was a Visiting Researcher at the Massachusetts Institute of Technology Sea Grant, Boston. His current research interests include nanonetworks and graphene-enabled wireless communication.

Mr. Jornet is a student member the Association for Computing Machinery.

Ian F. Akyildiz (F'96) received the B.S., M.S., and Ph.D. degrees in computer engineering from the University of Erlangen-Nürnberg, Germany, in 1978, 1981, and 1984, respectively. He is currently the Ken Byers Chair Professor with the School of Electrical and Computer Engineering, the Director of the Broadband Wireless Networking Laboratory, and the Chair of the Telecommunications Group at the Georgia Institute of Technology, Atlanta. In June 2008, he became an Honorary Professor with the School of Electrical Engineering, Universitat Politècnica de Catalunya in Barcelona, Spain. He is also the Director of the newly founded NaNoNetworking Center in Catalunya, Universitat Politècnica de Catalunya, Barcelona, Spain. He has also been an Honorary Professor with the University of Pretoria, South Africa, since March 2009. His research interests include in nanonetworks, cognitive radio networks, and wireless sensor networks.

Dr. Akyildiz is the Editor-in-Chief of *Computer Networks* (Elsevier) Journal, and the Founding Editor-in-Chief of the *Ad Hoc Networks* (Elsevier) Journal, *the Physical Communication* (Elsevier) Journal, and the *Nano Communication Networks* (Elsevier) Journal. He serves on the advisory boards of several research centers, journals, conferences, and publication companies. He became an Association for Computing Machinery (ACM) Fellow in 1997. He received numerous awards from the IEEE and ACM.